THE JOURNAL OF BIOLOGICAL CHEMISTRY
Vol. 279, No. 22, Issue of May 28, pp. 22809–22819, 2004

Printed in U.S.A.

Biosynthetic Ca^{2+}/Sr^{2+} Exchange in the Photosystem II Oxygen-evolving Enzyme of *Thermosynechococcus elongatus**[S]

Received for publication, February 16, 2004, and in revised form, February 27, 2004
Published, JBC Papers in Press, February 29, 2004, DOI 10.1074/jbc.M401677200

Alain Boussac‡§, Fabrice Rappaport¶, Patrick Carrier‖, Jean-Marc Verbavatz, Renée Gobin**, Diana Kirilovsky‡, A. William Rutherford‡, and Miwa Sugiura‡**

*From the ‡Service de Bioénergétique, DBJC, URA CNRS 2096, CEA Saclay, 91191 Gif sur Yvette, France, ¶Institut de Biologie Physico-Chimique, CNRS, UPR 1261, 13 rue Pierre et Marie Curie, 75005 Paris, France, ‖Laboratoire d'Ecologie de la Photosynthèse, DEVM, CEA Cadarache, 13108 Saint Paul lez Durance, France, and **Service de Biophysique des Fonctions Membranaires, DBJC, CEA Saclay, 91191 Gif sur Yvette, France*

The thermophilic cyanobacterium, *Thermosynechococcus elongatus*, has been grown in the presence of Sr^{2+} instead of Ca^{2+} with the aim of biosynthetically replacing the Ca^{2+} of the oxygen-evolving enzyme with Sr^{2+}. Not only were the cells able to grow normally with Sr^{2+}, they actively accumulated the ion to levels higher than those of Ca^{2+} in the normal cultures. A protocol was developed to purify a fully active Sr^{2+}-containing photosystem II (PSII). The modified enzyme contained a normal polypeptide profile and 1 strontium/4 manganese, indicating that the normal enzyme contains 1 calcium/4 manganese. The Sr^{2+}- and Ca^{2+}-containing enzymes were compared using EPR spectroscopy, UV-visible absorption spectroscopy, and O_2 polarography. The Ca^{2+}/Sr^{2+} exchange resulted in the modification of the EPR spectrum of the manganese cluster and a slower turnover of the redox cycle (the so-called S-state cycle), resulting in diminished O_2 evolution activity under continuous saturating light: all features reported previously by biochemical Ca^{2+}/Sr^{2+} exchange in plant PSII. This allays doubts that these changes could be because of secondary effects induced by the biochemical treatments themselves. In addition, the Sr^{2+}-containing PSII has other kinetics modifications: 1) it has an increased stability of the S_3 redox state; 2) it shows an increase in the rate of electron donation from Tyr_D, the redox-active tyrosine of the D_2 protein, to the oxygen-evolving complex in the S_3-state forming S_2; 3) the rate of oxidation of the S_0-state to the S_1-state by $Tyr_D^{\cdot}$ is increased; and 4) the release of O_2 is slowed down to an extent similar to that seen for the slowdown of the $S_3Tyr_Z^{\cdot}$ to S_0Tyr_Z transition, consistent with the latter constituting the limiting step of the water oxidation mechanism in Sr^{2+}-substituted enzyme as well as in the normal enzyme. The replacement of Ca^{2+} by Sr^{2+} appears to have multiple effects on kinetics properties of the enzyme that may be explained by S-state-dependent shifts in the redox properties of both the manganese complex and Tyr_Z as well as structural effects.

The evolution of oxygen as a result of light-driven water oxidation is catalyzed by photosystem II (PSII)[1] in which a cluster of 4 manganese ions acts both as a device for accumulating oxidizing equivalents and as the active site. The reaction center of PSII is made up of two membrane-spanning polypeptides (D1 and D2) that bear the redox cofactors involved in the main electron transfer route. Absorption of a photon results in a charge separation between a chlorophyll molecule (P_{680}), and a pheophytin molecule. The pheophytin anion transfers the electron to a quinone, Q_A, and P_{680}^{+} is reduced by a tyrosine residue, Tyr_Z, that in turn is reduced by the Mn_4 cluster. During the enzyme cycle, the oxidizing side of PSII goes through five different redox states that are denoted S_n, n varying from 0 to 4. Oxygen is released during the S_3 to S_0 transition in which S_4 is a transient state (reviewed in Refs. 1–4).

Ca^{2+} ions are known to be required for enzyme activity (1, 5–8). The role of Ca^{2+} in PSII oxygen evolution has been the focus of numerous articles in the last 20 years. Most of our knowledge on the role of Ca^{2+} comes from studies on plant PSII. In PSII from plants, 1 Ca^{2+} is associated with the chlorophyll-binding protein CP29 (9), a protein that is absent in cyanobacteria, and the second Ca^{2+} ion is required for water oxidation to take place (1, 5, 10–12). A specific binding site appears during the assembly of the Mn_4 cluster (6), and its replacement with Sr^{2+} perturbs the Mn_4 EPR properties (7). No other metal ions are able to reconstitute significant enzyme activity (1, 5, 8, 13). The reconstitution of Ca^{2+}-depleted plant PSII with Sr^{2+} restores approximately 40% of the oxygen evolution activity (7, 8, 14). This decreased activity is because of a slowdown of the S-state transitions (7, 14, 15).

When Ca^{2+} (or Sr^{2+}) is removed from its site, manganese oxidation can still take place allowing formation of S_2, but on the following step, the normal S_3-state is not formed (16, 17). Instead, an abnormally stable form of the $Tyr_Z^{\cdot}$ is generated (18, 19) that interacts magnetically with the manganese (still in the S_2-state) (16, 17). In addition, the rate of oxidation of Tyr_Z is slowed down by several orders of magnitude when Ca^{2+} is absent (Ref. 14, see also Refs. 20 and 21), suggesting a role for Ca^{2+} in the deprotonation of Tyr_Z. Other suggested roles for Ca^{2+} include: 1) controlling substrate and Cl^{-} access to the active site (22) and 2) acting as a substrate water site (23, 24). Such roles imply proximity to manganese ions and the Tyr as first indicated from Ca^{2+}/Sr^{2+} exchange experiments (7), and indeed recent EXAFS studies strongly favor a structural model in which Ca^{2+} is close to manganese or even within its coordination sphere (25, 26).

* The costs of publication of this article were defrayed in part by the payment of page charges. This article must therefore be hereby marked "*advertisement*" in accordance with 18 U.S.C. Section 1734 solely to indicate this fact.

[S] The on-line version of this article (available at http://www.jbc.org) contains Figures S1 and S2.

§ To whom correspondence should be addressed. Tel.: 33-1-69-08-72-06; Fax: 33 -1-69-08-87-17; E-mail: alain.boussac@cea.fr.

[1] The abbreviations used are: PSII, photosystem II; PSI, photosystem I; Chl, chlorophyll; EPR, electron paramagnetic resonance; ICP, inductively coupled plasma optical emission spectrometry; EXAFS, extended x-ray absorption fine structure; MES, 2-(*N*-morpholino)ethanesulfonic acid; CHES, 2-(*N*-cyclohexylamino)ethanesulfonic acid; PPBQ, phenyl-*p*-benzoquinone; DCBQ, 2,6-dichlorophenylbenzoquinone; Nd:YAG, neodymium:yttriumaluminum garnet; W, watt(s); J, joule(s); PBS, phosphate-buffered saline; β-DM, *n*-dodecyl-β-maltoside.

The replacement of Ca^{2+} with Sr^{2+} provides a relatively rare case in which the enzyme turns over in all the centers but is kinetically limited. This material is thus of particular interest for enzymological and spectroscopic studies. The effects of Ca^{2+}/Sr^{2+} exchange have been studied by continuous wave-EPR (7, 15, 16, 27) and pulsed-EPR (28), Fourier transform infrared spectroscopy (29, 30), and EXAFS (strontium, calcium and manganese EXAFS) (25, 26). From Fourier transform infrared spectroscopy measurements, it has been proposed that a Mn-O-Mn cluster vibrational mode is modified upon Ca^{2+} replacement by Sr^{2+} (29) and that Ca^{2+} could be necessary for the formation of the hydrogen bond network involved in the reaction step of water oxidation (30). From the strontium-EXAFS done on Sr^{2+}-reconstituted Ca^{2+}-depleted PSII, a manganese-strontium distance of 3.4 Å has been proposed (25) (a value confirmed by calcium-EXAFS done on normal PSII sample (Ref. 26)). In addition, it was found by mass spectrometry experiments that substitution of Ca^{2+} by Sr^{2+} accelerated the slow rate of $H_2{}^{18}O$ exchange by a factor of 3–4 in the S_1-, S_2-, and S_3-states (31).

These experiments were all performed after appropriate biochemical treatments leading to Ca^{2+}/Sr^{2+} exchange. In general, these treatments consist of washing PSII in high salt buffers in the light (at pH 6.5, Ca^{2+}/Sr^{2+} exchange occurred in the S_3-state) (7, 16) or by treatment at low pHs (≤3) (32). Doubts have been raised in the past concerning potential secondary effects of the biochemical treatments used, and it has been suggested that some of the phenomena associated with Ca^{2+} depletion, and by implication Sr^{2+} replacement, may be because of secondary structural effects (1, 5, 10, 33, 34). Although good arguments have been made to counter these doubts (1, 10, 35), these have been revived by related work focused on removal and exchange of chloride ions where secondary biochemical effects have been specifically invoked (36).

The procedures to remove Ca^{2+} always result in an inhibition (*i.e.* the release of the Mn_4 cluster) of a small proportion of PSII centers (37, 38). In addition, Sr^{2+} reconstitution is not necessarily 100% efficient and the Sr^{2+}-reconstituted PSII is very often an unstable material. All of these effects rendered the previous Sr^{2+}-reconstituted PSII an heterogeneous enzyme. These have made imperative the development of a new fully stable and fully active strontium-PSII.

The focus of PSII research recently has turned to cyanobacterial PSII because of 1) the availability of mutants (39–41) and 2) a move to study thermophilic species of cyanobacteria that have provided excellent spectroscopic material (27, 42–45) and have provided the first x-ray crystallographic models of PSII (46, 47). The role of Ca^{2+} in cyanobacterial PSII is more poorly understood than in plant systems. From a few studies, a less specific ion requirement has been reported (33, 48), and the biochemical procedures developed for Ca^{2+} ion removal in plants are inappropriate for cyanobacterial systems, because of differences in the extrinsic polypeptides present in cyanobacteria compared with plants (*e.g.* Refs. 3 and 49).

The measurement of calcium stoichiometries in PSII has proved particularly problematic. Because of the ubiquitous nature of Ca^{2+}, background levels are often close to the concentration found in the biological samples. Many years of wrangling went on before the field stopped arguing over the stoichiometry in plant material (10, 11, 35). To measure the stoichiometry of calcium in PSII of cyanobacteria, we wished to avoid the difficulties encountered in plant PSII. One approach that seemed worth trying was the biosynthetic replacement of Ca^{2+} with Sr^{2+} by growing the cyanobacterial cells in Sr^{2+}-containing media. This approach promised the benefit of providing material not only for the measurement of strontium (and hence calcium) stoichiometries, but also for enzymological and spectroscopic studies in cyanobacteria without the necessity of developing the exchange procedures *in vitro* and without the risk of preparation artifacts.

Here we present (*a*) the results of this biosynthetic replacement study using *Thermosynechococcus elongatus,* (*b*) a procedure for the isolation of the Sr^{2+}-containing enzyme, and (*c*) the results of kinetics and enzymological studies.

EXPERIMENTAL PROCEDURES

Purification of "Thylakoids" and PSII Core Complexes—T. elongatus (43-H strain) (41) were grown in 3-liter Erlenmeyer flasks (1500-ml culture) in a rotary shaker (120 rpm) at 45 °C under continuous illumination from fluorescent white lamps (≈80 μmol of photons·m^{-2}·s^{-1}). The cells were grown in a DTN medium (41) containing either 0.8 mM $CaCl_2$ or 0.8 mM $SrCl_2$ in an CO_2-enriched atmosphere. Cells were grown until they reached an optical density (OD) close to 1.0 at 800 nm. After harvesting by centrifugation, the cells were washed once with buffer 1 (40 mM MES, pH 6.5, 15 mM $MgCl_2$, 15 mM $CaCl_2$, 10% glycerol, 1.2 M betaine) and resuspended in the same buffer, with 0.2% (w/v) bovine serum albumin, 1 mM benzamidine, 1 mM aminocaproic acid, and 50 μg·ml^{-1} DNase I added, to a chlorophyll concentration of ≈1.5 mg·ml^{-1}. The cells were ruptured with a French press (≈700 p.s.i.). Unbroken cells were removed by centrifugation (1,000 × *g*, 5 min). Thylakoids were pelleted by centrifugation at 180,000 × *g* for 35 min at 4 °C and washed twice with buffer 1. Thylakoids were finally resuspended in buffer 1 and stored in liquid N_2 at a Chl concentration of 1 mg·ml^{-1} before use. Thylakoids obtained from cells grown in the presence of either Ca^{2+} or Sr^{2+} will be noted as Ca-thylakoids or Sr-thylakoids, respectively.

PSII were purified from freshly prepared thylakoids essentially as described previously (41) but with the following modifications. Thylakoids (1 mg·ml^{-1}, final concentration) were treated with 1% (w/v) *n*-dodecyl-β-maltoside (β-DM, Biomol, Germany) in buffer 1 supplemented with 100 mM NaCl. After ≈1 min of stirring in the dark at 4 °C the suspension was centrifuged (10 min, 170,000 × *g*) to remove the non-solubilized material. Then, the supernatant was mixed with an equal volume of Probond resin (Invitrogen, Groningen, The Netherlands) that had been pre-equilibrated with buffer 1. The resulting slurry was transferred to an empty column. After sedimentation of the resin inside the column, the supernatant was removed. The resin was washed with buffer 2 (40 mM MES, 15 mM $MgCl_2$, 15 mM $CaCl_2$, 100 mM NaCl, 15 mM imidazole, 0.03% (w/v) β-DM, 10% (v/v) glycerol, 1.2 M betaine, pH 6.5) until the OD value of the eluate at ≈670 nm decreased below 0.05. Then, PSII core complexes were eluted with buffer 3 (150 mM MES, 15 mM $MgCl_2$, 15 mM $CaCl_2$, 200 mM NaCl, 300 mM imidazole, 0.1% (w/v) β-DM, 10% (v/v) glycerol, 1.2 M betaine, the pH was adjusted to 6.5 by adding concentrated HCl). The eluate was then either precipitated with buffer 1 with 15% (w/v) polyethylene glycol-8000 added by centrifugation (10 min, 170,000 × *g*) or concentrated and washed using centrifugal filter devices (Ultrafree-15, Millipore). PSII core complexes were finally resuspended in buffer 1 at a Chl concentration of 1–1.5 mg·ml^{-1} and store in liquid N_2 before to be used. The estimate of Chl concentration was done by solubilizing the biological material in methanol and by using an extinction coefficient equal to 79.95 mg^{-1}·ml·cm^{-1} at 665 nm (51). PSII core complexes purified from cells grown in the presence of either Ca^{2+} or Sr^{2+} will be noted calcium-PSII or strontium-PSII, respectively.

Manganese Depletion—Manganese depletion of PSII was done by a washing of the sample in 1.2 M Tris, pH 9.2, in room light at 4 °C for 1 h. After centrifugation (3 h, 170,000 × *g*), the pellet was submitted to a second washing in 1 M $CaCl_2$ for 30 min at 4 °C. PSII depleted of the manganese cluster and of the three extrinsic proteins was then pelleted by centrifugation (3 h, 170,000 × *g*) and resuspended in buffer 1.

Sodium Dodecyl Sulfate-Polyacrylamide Gel Electrophoresis—Calcium-PSII, strontium-PSII, and manganese-depleted PSII were mixed with 30 mM Tris, pH 8.5, 30 mM dithiothreitol, and 1% lauryl sulfate at a Chl concentration of 0.5 mg·ml^{-1}. Samples were incubated on ice for 10 min and then applied to a 16–22% gradient of SDS-polyacrylamide gel containing 7.5 M urea (52). Electrophoresis was done under a current of 10 mA. The gel was stained with Coomassie Brilliant Blue as described previously (52).

Oxygen Evolution Measurements—Oxygen evolution under continuous light was measured at 25 °C by polarography using a Clark-type oxygen electrode (Hansatech) with saturating white light. Oxygen evolution of PSII core complexes (5 μg of Chl·ml^{-1}) was measured in buffer

TABLE I
Metals content in whole T. elongatus cells grown in the presence of 0.8 mM Ca^{2+}, 0.8 mM Sr^{2+}, or both 0.4 mM Ca^{2+} and 0.4 mM Sr^{2+}

	Ca/Chl	Sr/Chl	Mn/Chl	Fe/Chl
Cells + 0.8 mM Ca^{2+}	8	0.001	0.016	0.37
Cells + 0.8 mM Sr^{2+}	0.1	23	0.014	0.35
Cells + 0.4 mM Ca^{2+} + 0.4 mM Sr^{2+}	4.5	16	0.018	0.43

1 in the presence of 0.5 mM DCBQ (2,6-dichloro-*p*-benzoquinone, dissolved in Me_2SO) or 0.5 mM PPBQ (phenyl-*p*-benzoquinone dissolved in Me_2SO) as electron acceptors. For measurements at various pH values, the following buffers were used: MES, pH 5.5, 6.0, and 6.5; HEPES, pH 7.0 and 7.5; CHES, pH 8.0 and 8.5.

Oxygen evolution under flashing light was measured with a laboratory-made rate electrode similar to that already described (53). Ca-thylakoids or Sr-thylakoids were used at 1 mg·ml^{-1} without an added electron acceptor. Illumination was done with a xenon flash. The power of the xenon flash was adjusted so that the light intensity was saturating (*i.e.* the miss parameter was minimum). Measurements were done at room temperature (20–25 °C). The flash-induced oxygen evolution patterns reported here were obtained as follows; the direct current was recorded with a numerical oscilloscope (see the *inset* to Fig. 8), and then the derivative *versus* time was computed mathematically. The derivative step (dt) used was dt = 10 ms for Ca-thylakoids and dt = 20 ms for Sr-thylakoids because the oxygen release was slower in Sr-thylakoids than in Ca-thylakoids. Then, the amplitude of the derivative signal was plotted *versus* the flash number. Analysis of the flash-induced oxygen evolution patterns was done using the classic equations listed below assuming the miss (α) and double hit (β) parameters to be equal on all flashes.

$$[O_2]_n = (1 - \alpha)[S_3]_{n-1} + \beta[S_2]_{n-1} \quad \text{(Eq. 1)}$$

$[O_2]_n$ is the amount of O_2 evolved after flash n, and $[S_3]_{n-1}$ and $[S_2]_{n-1}$ are the amount of S_3 and S_2, respectively, before flash n.

$$[S_i]_n = (1 - \alpha - \beta)[S_{i-1}]_{n-1} + \beta[S_{i-2}]_{n-1} + \alpha[S_i]_{n-1} \quad \text{(Eq. 2)}$$

A scaling factor multiplying the experimental data was introduced into the fitting procedure so that the amount of O_2 evolved upon each flash corresponded to the percentage of centers by which it was produced.

Continuous Wave-EPR Measurements—CW-EPR spectra were recorded using a standard ER 4102 (Bruker) X-band resonator with a Bruker ESP300 X-band spectrometer equipped with an Oxford Instruments cryostat (ESR 900). Continuous illumination of the Sr-thylakoid samples ([Chl] ≈ 3–4 mg·ml^{-1}) was done with an 800-W tungsten lamp, light from which was filtered through water and IR filters, in a nonsilvered Dewar flask filled with ethanol cooled to 198 K with solid CO_2. Flash illumination at room temperature was provided by a Nd:YAG laser (532 nm, 550 mJ, 8 ns Spectra Physics GCR-230-10). For measurements of the S_2-multiline signal after a given number of flashes, strontium-PSII samples at 1 mg·ml^{-1} were loaded in the dark into quartz EPR tubes and further dark-adapted for 1 h at room temperature. Then, the strontium-PSII samples were synchronized in the S_1-state with one pre-flash (27). After another dark period of 1 h at room temperature, 1 mM phenyl-*p*-benzoquinone dissolved in Me_2SO was added (the final concentration of Me_2SO was ≈3%). After illumination by the indicated number of flashes, the samples were frozen in the dark to 198 K, degassed at 198 K as already described (54), and then transferred to 77 K. For the measurements of $Tyr_Z^{\bullet}$ formation and decay at room temperature, calcium-PSII and strontium-PSII samples ([Chl] = 1 mg·ml^{-1}) were loaded into a flat cell and then illuminated directly in the EPR cavity with the Nd:YAG laser describe above. The power of the laser was decreased to ≈200 mW, which was strong enough to saturate the samples. Scaling of the different traces was carefully done using the Chl concentration of the samples. A check of the reaction center concentration has also been done using the $Tyr_D^{\bullet}$ signal amplitude as an internal EPR probe. The amplitude of the $Tyr_D^{\bullet}$ signal was measured after the last flash of the series, assuming that in these conditions $Tyr_D^{\bullet}$ was oxidized in all centers.

Near-IR illumination of the samples was done directly in the EPR cavity and was provided by a laser diode emitting at 820 nm (Coherent, diode S-81-1000C) with a power of 600–700 mW at the level of the sample.

UV-visible Absorption Changes—Absorption changes were measured with a laboratory-built spectrophotometer (55), where the absorption changes are sampled at discrete times by short flashes. These flashes are provided by a Nd:YAG pumped (355 nm) optical parametric oscillator, which produces monochromatic flashes (1 nm full-width at half-maximum) with a duration of 6 ns. Excitation was provided by a dye laser pumped by the second harmonic of a Nd:YAG laser (685 nm, 1 mJ). PSII cores complexes were used at 25 μg of Chl·ml^{-1} in buffer 1. After dark adaptation for 1 h at room temperature (20–22 °C), 0.1 mM PPBQ was added as an electron acceptor. DCBQ could not be used in this experiment because it became reduced in the minutes time scale in the presence of betaine (data not shown).

Measurements of Metal Contents—The metal contents were determined by inductively coupled plasma optical emission spectrometry (ICP) (Vista-MPX CCD Simultaneous ICP-OES; Varian, Australia) (56). Samples were mineralized overnight at room temperature in concentrated HNO_3 (>69.5%, TraceSelect, Fluka). Then, the samples were diluted with 18 MΩ water so that the acid concentration was below 5%. For metal content analysis in whole cells, the cells were grown in the same conditions with either 0.8 mM $CaCl_2$ or 0.8 mM $SrCl_2$ or both 0.4 mM $CaCl_2$ and 0.4 mM $SrCl_2$. Harvesting of the cells was done when they reached an OD of 0.9 at 800 nm. They were then washed twice by centrifugation (5 min, 4000 × g) and resuspension in a large volume of water containing 100 μM EGTA (pH 7) at 4 °C to remove the metals bound on the surface of the cells.

Electron Microscopy—Cells were centrifuged and resuspended in fixative phosphate-buffered saline (PBS) at pH 7.4 and containing 2% glutaraldehyde and incubated overnight at 4 °C. Then, the cells were incubated for 10 min in PBS, harvested by centrifugation, resuspended in PBS, and incubated for another 24 h. Then, after harvesting by centrifugation, the cells were washed twice (by suspension and centrifugation steps) in water and incubated for 15 min in 1% sodium metaperiodate. The cells were post-fixed for 1 h in 1% sodium tetroxide and 1.5% potassium ferrocyanide in water (57). Automated Epon embedding was carried out after dehydration in graded concentrations of ethanol (70–100%) in a Leica Lynx apparatus. Thin sections were cut on a Leica ultramicrotome, collected on copper grids, counterstained with Reynold's lead citrate, and photographed at the electron microscope (Philips EM 400) at 80 kV.

RESULTS

The ability for *T. elongatus* cells to grow with Sr^{2+}-salt instead of Ca^{2+}-salt was tested by comparing the growth curves in the presence of either Ca^{2+} or Sr^{2+} in the culture medium. The concentration of the cells was estimated by measuring the diffusion of light at 800 nm. In the exponential phase, a similar doubling time close to 15 h was observed under both conditions. By contrast, without the addition of either the Ca^{2+} or the Sr^{2+} ion in the culture medium, the cells did not grow (data not shown, but see Supplementary Material available in the on-line version of this article).

In some cyanobacteria, it has been reported that an increase of the strontium ion in the environment induced some perturbations as the formation of external vesicles (58, 59). We looked for such effects in the ultrastructure of *T. elongatus* grown in the presence of Sr^{2+} because we thought such effects could be responsible for the difficulties encountered in isolating active strontium-PSII (see below). At the resolution used, the photosynthetic membranes appeared to be similar in both types of cells (data not shown, but see Supplementary Material available in the on-line version of this article).

The metals content in whole cells was analyzed by ICP spectroscopy. The values are listed in Table I. They are expressed as the ratio "number of metal per 1 Chl." The presence of either Ca^{2+} or Sr^{2+} in the culture media did not strongly affect the manganese and iron contents in the cells. By contrast, the strontium level in cells cultivated in the presence of Sr^{2+} was much higher than the calcium level in cells cultivated

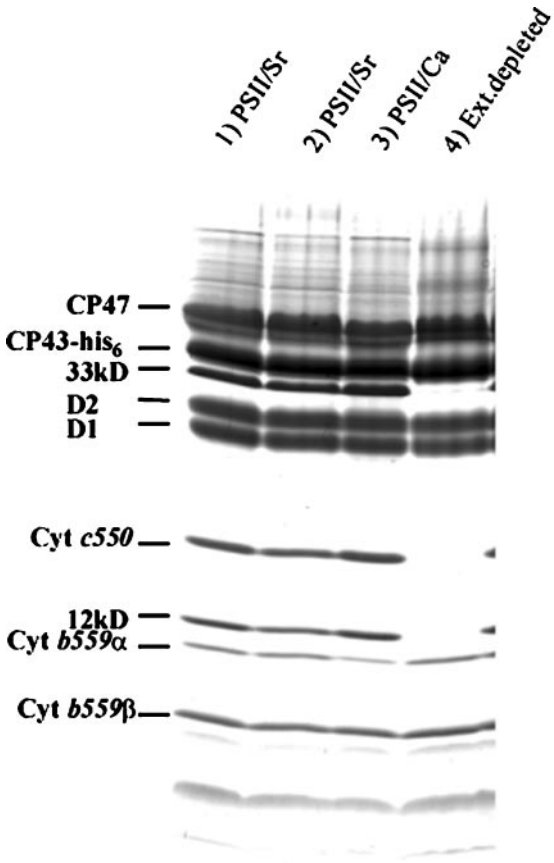

FIG. 1. **Coomassie Brilliant Blue staining of SDS-PAGE of purified strontium-PSII (*lanes 1* and *2*), calcium-PSII (*lane 3*), and PSII depleted of the three extrinsic polypeptides (*lane 4*).** 10 μg of Chl was loaded in each lane. See "Experimental Procedures" for additional details.

in the presence of Ca^{2+}. This result shows that *T. elongatus* accumulates more (~4 times in these conditions) strontium than calcium. When cells were cultivated with both Ca^{2+} and Sr^{2+} in the medium, they still accumulate strontium.

Our first attempts to purify fully active oxygen-evolving PSII using the protocol developed for normal cells failed. From EPR spectroscopy it appeared that the oxidized cytochrome *c*-550 was no longer bound to PSII (given the very low potential of this cytochrome (60) the loss of the Fe^{3+} EPR signal being caused by its reduction seems unlikely). This indicated that the replacement of Ca^{2+} by Sr^{2+} decreased the affinity of PSII for this extrinsic PSII subunit. Because the loss of the cytochrome *c*-550 is often accompanied by the loss of the other extrinsic proteins and hence by the loss of the Mn_4 cluster, it seemed likely that this was related to the lack of activity. Several different approaches were tested to isolate active strontium-PSII; these included the addition of high amount of glycerol and/or mannitol, breaking of the cells with glass beads instead of the French press, etc. Eventually, we found that the addition of $\geq$1 M betaine in the buffers was sufficient to obtain active strontium-PSII. Betaine has already been shown to protect PSII against several stresses and, more precisely, against those inducing the release of the extrinsic proteins (see Ref. 61 and references therein).

Fig. 1 shows the electrophoretic profile of two different strontium-PSII preparations (*lanes 1* and *2*), of calcium-PSII (*lane 3*) (all purified in the presence of betaine; see "Experimental Procedures"), and of calcium-PSII from which the 33-kDa, 12-kDa, and cytochrome c_{550} subunits have been removed by a Tris washing, followed by a $CaCl_2$ washing (*lane 4*). Fig. 1 shows that the polypeptide content (in particular the 33-kDa, 12-kDa, and cytochrome c_{550} extrinsic subunits) was similar in calcium-PSII and strontium-PSII.

The measurement of manganese and strontium contents by ICP on three different strontium-PSII batches gave a strontium/4 manganese ratio of 1.05 $\pm$ 0.10. Because strontium-PSII was purified in the presence of 15 mM Ca^{2+} in all buffers, any exchangeable Sr^{2+} ions either specifically or nonspecifically bound to PSII were expected to be efficiently exchanged with Ca^{2+} from the buffer. Assuming 4 manganese/PSII reaction center, we may conclude that our strontium-PSII preparation contained 1 Sr^{2+}/PSII reaction center. As, from the results presented below, the proportion of inactive centers resulting from empty Sr^{2+} sites is very probably negligible, it can be concluded that there is 1 Sr^{2+}, and therefore 1 Ca^{2+}, per PSII reaction center in PSII from *T. elongatus*.

The manganese per PSII reaction center ratio may also be deduced from the chlorophyll concentration of the sample used for ICP measurements. By doing such an estimate, we found 43 Chls/4 manganese in calcium-PSII. Such a ratio is higher than that deduced from three-dimensional crystallography (*i.e.* 35 Chls/4 manganese (Refs. 46 and 50) and 36 Chls/4 manganese (Ref. 47)). However, our preparation conditions are milder than those used in the crystallography studies; thus, any weakly or nonspecifically bound chlorophylls are more likely to have been removed in the material used for crystallography (46, 47, 50). A value of 39 Chls/reaction center has also been reported in highly active PSII from *T. elongatus* (62).

In addition to the manganese and strontium contents, we also measured the iron content in calcium-PSII and strontium-PSII and found a value of 3.7 $\pm$ 0.3 iron/4 manganese. This value is close to the expected value of 3 (1 iron for the non-heme iron, 1 iron for cytochrome C-550, and 1 iron for cytochrome b_{559}). By EPR, a contaminant high spin Fe^{III} is always found in PSII samples (see for example the signal at g = 4.3, *i.e.* at $\approx$1600 gauss, in Fig. 3). This could account for the extra 0.7 $\pm$ 0.3 iron/4 manganese detected here by ICP.

Biochemical exchange of Ca^{2+} by Sr^{2+} is known to affect the EPR properties of the Mn_4 cluster in the S_2-state similarly in PSII from plants (7) and PSII from *T. elongatus* (27). Therefore, this spectroscopic probe was used to confirm that Sr^{2+} has replaced Ca^{2+}. The EPR experiment was first performed on Sr-thylakoids. The membrane suspension was put into an EPR tube and dark-adapted for 1 h at room temperature to obtain PSII mainly in the S_1-state. Then the sample was frozen to 198 K before illumination at this temperature to form the S_2-state in most of the centers. The EPR spectrum of such a sample is complicated because of the presence of many EPR signals originating from PSI and from other membrane-associated complexes (data not shown). This complexity made difficult the characterization of the S_2-multiline signal. To overcome this difficulty, after the 198 K illumination, the sample was further illuminated by a 820 nm light, at 50 K, in the EPR cavity. This near-infrared illumination has been shown to convert the spin 1/2 S_2-multiline signal state into an S $\geq$ 5/2 spin state characterized by signals around g = 9 (44). The difference signal before *minus* after the 820 nm illumination is shown in Fig. 2 (*spectrum b*). This corresponds to the S_2-multiline signal, which disappeared upon near infrared illumination. This S_2-multiline signal is clearly different from a normal S_2-multiline signal (*spectrum a*) and exhibits the characteristic number of lines and the line spacing observed in Sr^{2+}-reconstitued PSII (7, 27). This experiment shows that Sr^{2+} bound to the same site as that in Sr^{2+}-reconstituted, Ca^{2+}-depleted PSII. Additionally, this result also shows that the previously reported modifications of the S_2-multiline in Sr^{2+}-reconstituted PSII are not caused by

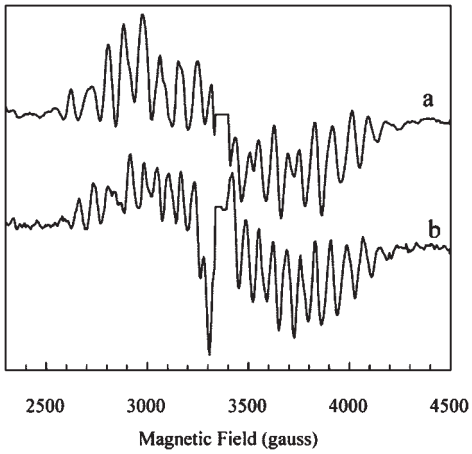

FIG. 2. **Effect of near-infrared light in the S_2-state of Sr-thylakoids.** *Spectrum a* corresponds to a normal S_2-multiline EPR spectrum recorded in calcium-PSII (27). *Spectrum b* corresponds to a difference spectrum obtained by subtracting the spectrum recorded after a 820-nm illumination at 50 K to that recorded before the near-infrared illumination in Sr-thylakoids. Temperature, 9 K; modulation amplitude, 25 gauss; microwave power, 20 mW; microwave frequency, 9.4 GHz; modulation frequency, 100 kHz. The central part of the spectra corresponding to the $Tyr_D^{\cdot}$ region was deleted.

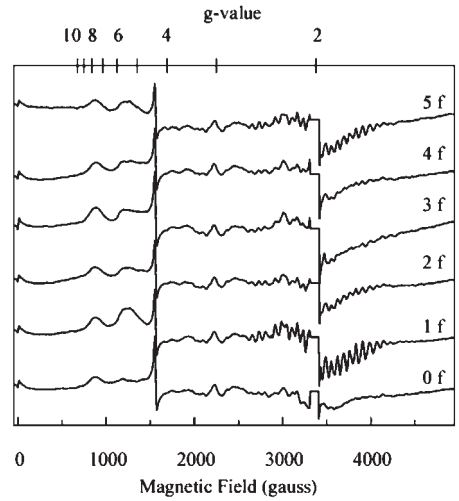

FIG. 3. **EPR spectra recorded on strontium-PSII (Chl ≈ 1 mg/ml) after a series of saturating laser flashes (1 Hz) in the presence of 1 mM PPBQ.** Instrument settings: modulation amplitude, 25 G; microwave power, 20 mW; microwave frequency, 9.4 GHz; modulation frequency, 100 kHz. Temperature, 9 K. The central part of the spectra corresponding to the $Tyr_D^{\cdot}$ region was deleted.

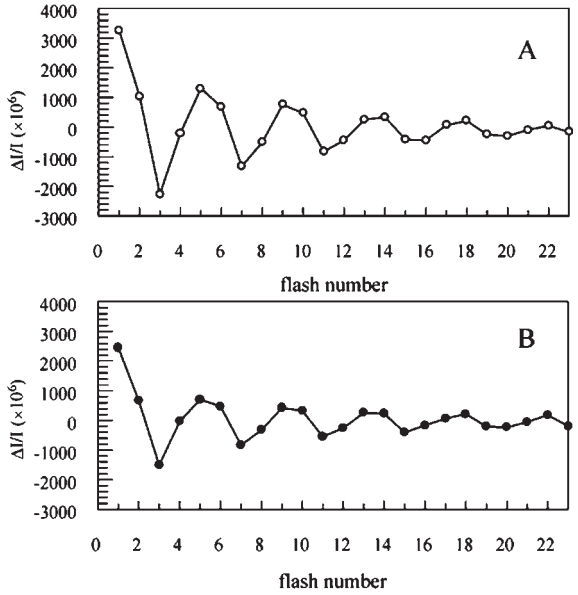

FIG. 4. **Sequence of the amplitude of the absorption changes at 292 nm during a series of saturating flashes (spaced 400 ms apart) given on calcium-PSII (*panel A*) and strontium-PSII (*panel B*).** The samples (Chl = 25 μg/ml) were dark-adapted for 1 h at room temperature before the addition of 100 μM PPBQ (dissolved in Me_2SO). The measurements were done 300 ms after each flash.

secondary effects of the biochemical treatment used to substitute Ca^{2+} for Sr^{2+}.

Fig. 3 shows the EPR spectra using strontium-PSII after illumination by the indicated number of flashes given at room temperature. In strontium-PSII, the multiline signal (between ≈2500 and ≈4300 gauss) observed after one flash, *i.e.* in the S_2-state, is similar to that previously observed in Sr^{2+}-reconstituted, Ca^{2+}-depleted PSII (27). Additional features in Fig. 3 are the following: 1) the g_z and g_y resonances of cytochrome c_{550} at ≈2230 gauss and ≈2920 gauss respectively (60), 2) a signal at g = 4.3 (≈1600 gauss) from a contaminant Fe^{III}, 3) the amplitude of the signals at g = 7.6 and g = 5.5, originating from the oxidized non-heme iron, oscillates with a period of 2 resulting from oxidation of the Fe^{2+} by the semiquinone form of PPBQ on the odd-numbered flashes, followed by reduction of Fe^{3+} by Q_A^- on even-numbered flashes (63).

Sr^{2+} reconstitution of Ca^{2+}-depleted plant PSII restores approximately 40% of the oxygen evolution activity when measured under continuous illumination (7, 8). This decrease in the activity has been shown to result from slower S-state transitions (14, 15). The half-time for the $S_3Tyr_Z^{\cdot}$ to S_0Tyr_Z transition was 5 ms after reconstitution of Ca^{2+}-depleted PSII with Ca^{2+} and 18 ms after reconstitution with Sr^{2+} (15). To determine the kinetics of the $S_iTyr_Z^{\cdot}$ to $S_{i+1}Tyr_Z$ transitions, we followed the absorption changes at 292 nm using a Joliot type spectrophotometer (64, 65). This wavelength corresponds to an isosbestic point for $PPBQ^-$/PPBQ (data not shown) and is in a spectral region where the absorption of the Mn_4 depends on the S-states. Therefore, (i) the amplitude of the absorption changes upon flash illumination in the hundreds of milliseconds time range (*i.e.* when reduction of $Tyr_Z^{\cdot}$ by the Mn_4 complex was completed) showed an oscillated pattern reflecting the S-state cycle and (ii) the kinetics of the absorption changes upon flash illumination in the nanoseconds to milliseconds time range are a measure of the $S_iTyr_Z^{\cdot}$ to $S_{i+1}Tyr_Z$ transitions (at least those in which the $\Delta I/I$ for Mn_4 oxidation is different from that of $Tyr_Z^{\cdot}/Tyr_Z$ *i.e.* the S_1 to S_2 and S_3 to S_0 transitions).

Fig. 4 shows the oscillating pattern observed with calcium-PSII (*panel A*) and strontium-PSII (*panel B*). Period four oscillations are clearly visible at least until the 23rd flash. For technical reasons the analytic flash had a small actinic effect. To partially take into account this effect, the data were fitted using a double hit parameter different from zero. The two parameters, α (miss) and β (double hit), can be calculated without the knowledge of the individual $\Delta\epsilon$ for each S-state transition (64). Using the formula developed by Lavorel (66) and the oscillating patterns in Fig. 4, the following values were obtained: in calcium-PSII, α = 8% and β = 4%; and in strontium-PSII, α = 7% and β = 3%. These values are similar showing no strong effect of Sr^{2+} substitution on the oscillating properties. The amplitude of the absorption changes associated with each flash of a series seem slightly smaller in strontium-PSII compared with calcium-PSII. This may reflect either a lower proportion of active centers (but see below) or different $\Delta\epsilon$ for some (or all) S-state transitions. This latter possibility is not unlikely if the Ca^{2+} ion, and therefore the Sr^{2+} ion, constitutes one of the four metals in the distorted cubane (50). Indeed, the

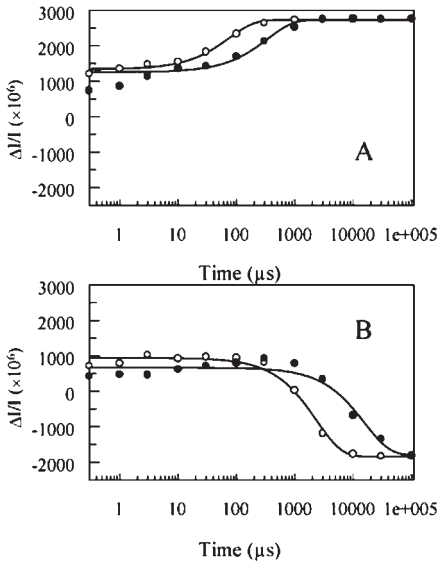

FIG. 5. **Kinetics of the absorption changes at 292 nm after the first flash (*panel A*) or the third flash (*panel B*) given on dark-adapted calcium-PSII (*open circles*) or strontium-PSII (*filled circles*).** Other experimental conditions were similar to those in Fig. 4.

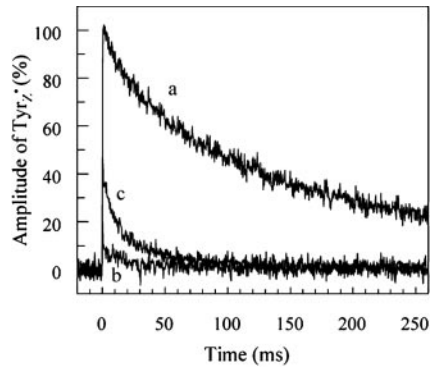

FIG. 6. **Formation and decay kinetics at room temperature of the $Tyr_Z^{\cdot}$ EPR signal recorded at 3340 G (at the position of the low field maximum of the $Tyr_Z^{\cdot}$ EPR spectrum) under repetitive flash experiment (spaced 5 s apart) in the presence of 0.5 mM PPBQ (dissolved in Me_2SO).** Each sample was submitted to 64 flashes. Then data from four samples were averaged. *Trace a* was recorded on manganese-depleted PSII. *Traces b* and *c* were measured on calcium-PSII and strontium-PSII, respectively. Chl = 1 mg/ml. Other experimental conditions were as follows: microwave power, 20 mW; modulation amplitude, 4.5 gauss; modulation frequency, 100 kHz; microwave frequency, 9.4 GHz; time constant, 0.32 ms.

metal exchange is expected to have some consequences on the structure and therefore on the spectral characteristics of the complex.

Fig. 5 reports the absorption changes at 292 nm from the nanosecond time scale to the millisecond time scale calcium-PSII (*open symbols*) and strontium-PSII (*closed symbols*). The results shown only concern the kinetics recorded after the first flash (*panel A*) and the third flash (*panel B*), which, to a first approximation, corresponded to the $S_1Tyr_Z^{\cdot}$ to S_2Tyr_Z and to the $S_3Tyr_Z^{\cdot}$ to S_0Tyr_Z transitions, respectively. In principle, we would have to remove small contributions from other S-state transitions after the first and third flash. However, we have observed that after the second and fourth flash (*i.e.* mainly for the S_2 to S_3 and S_0 to S_1 transitions) the $\Delta I/I$ of the $Tyr_Z^{\cdot} \rightarrow Tyr_Z$ and $S_{i \rightarrow Si+1}$ transitions were similar at 292 nm. This has two consequences: 1) the electron transfer kinetics for the S_0 to S_1 and S_2 to S_3 transitions cannot be monitored at 292 nm, and 2) the S_0 to S_1 and S_2 to S_3 transitions do not contribute significantly to the absorption changes detected at 292 nm after the first and third flash.

The $S_1Tyr_Z^{\cdot}$ to S_2Tyr_Z transition was slowed down from 50 to 230 μs and the $S_3Tyr_Z^{\cdot}$ to S_0Tyr_Z transition was slowed down from 1.6 to 11 ms. The $t_{1/2}$ found in this work for calcium-PSII are similar to those reported previously (65, 67). By contrast, the S_3 $Tyr_Z^{\cdot}$ to S_0Tyr_Z and $S_1Tyr_Z^{\cdot}$ to S_2Tyr_Z transitions in strontium-PSII are significantly faster than those reported previously for Sr^{2+}-reconstituted Ca^{2+}-depleted PSII (15). A possible reason for that is the absence of the 24-kDa polypeptide in the previous EPR work (15). Indeed, in PSII from plants the removal of this protein increases the half-time of the $S_3Tyr_Z^{\cdot}$ to S_0Tyr_Z transition from 1 to 5 ms (68). The following observations can also be made from the data in Fig. 5. Although in calcium-PSII the $\Delta I/I$ did not vary significantly in the 1–10-μs time range after the flash, in strontium-PSII we observed a small increase. Such an effect could reflect a slower equilibration rate for the $Tyr_ZP^+ \leftrightarrow Tyr_Z^{\cdot}P$ equilibrium in strontium-PSII compared with calcium-PSII.

In the absence of the Mn_4 cluster, $Tyr_Z^{\cdot}$ reduction is expected to occur in the tens to hundreds of milliseconds time scale (69). From results reported in Fig. 5, there is no evidence for such very slow kinetics in strontium-PSII. This would indicate that the sample contained no detectable amount of PSII centers inactive in oxygen evolution. To further support this conclusion, we have measured $Tyr_Z^{\cdot}$ formation and reduction upon repetitive flash illumination by using EPR spectroscopy (Fig. 6). This technique allows the detection of the $Tyr_Z^{\cdot}$ radical without any other contributions except that from $Tyr_D^{\cdot}$, which can be considered as stable in the time scale where $Tyr_Z^{\cdot}$ is re-reduced. The $Tyr_Z^{\cdot}$ formation and reduction was first measured in the manganese-depleted sample (*trace a*). The amplitude of the signal has been arbitrarily scaled to 100%. The decay of *trace a* is bi-exponential, 72% of $Tyr_Z^{\cdot}$ decayed with a $t_{1/2}$ = 150 ms and 28% with a $t_{1/2}$ = 22 ms. *Trace b* was measured in calcium-PSII. In this sample the reduction of $Tyr_Z^{\cdot}$ is too fast ($t_{1/2} \leq$ 1.6 ms from data in Fig. 5) to be measured in our EPR conditions. We could only detect the tail of the decay of the slowest S-state transition, *i.e.* the $S_3Tyr_Z^{\cdot}$ to S_0Tyr_Z transition with $t_{1/2}$ = 1.6 ms. *Trace c* was measured in strontium-PSII. The maximum signal amplitude corresponded to ≈40% of *trace a*. Because *trace c* results from the average of all S-state transitions, only those in which the $t_{1/2}$ is >1 ms can be detected and each would be expected to be 25% of the signal amplitude in *trace a* if fully resolved.

It is difficult to obtain a very satisfactory fit of *trace c* (data not shown). A relatively good fit may include a component corresponding to ≈5–10% of *trace a*. This percentage would correspond to an upper limit for inactive centers. The remaining part of *trace c* corresponded to 25–30% of the centers. In this phase, $Tyr_Z^{\cdot}$ decayed with a $t_{1/2}$ equal to 10 ms. The amplitude of the 10-ms phase is close to the maximum amount of $Tyr_Z^{\cdot}$, which can be detected if only one S-state transition contributes to the signal. The $t_{1/2}$ of this phase is very close to that of the $S_3Tyr_Z^{\cdot}$ to S_0Tyr_Z transition already detected at 292 nm in Fig. 5. *Trace c* also contains a phase faster than the time resolution of the spectrometer (amplitude of which corresponds approximately to 5% of the centers). This short-lived signal could correspond to the tail of the $S_2Tyr_Z^{\cdot}$ to S_3Tyr_Z transition, *i.e.* the second slowest transition (15).

In PSII from plants the oxygen evolution activity under continuous saturating light, at pH 6.5, was decreased by a factor of ≈2.5 after a Ca^{2+}/Sr^{2+} exchange (7, 8). We report here an experiment in which O_2 evolution was measured in calcium-PSII and strontium-PSII. Because the pH value and/or the type of electron acceptor may differently affect the activity in calcium-PSII and strontium-PSII, measurements were done as a

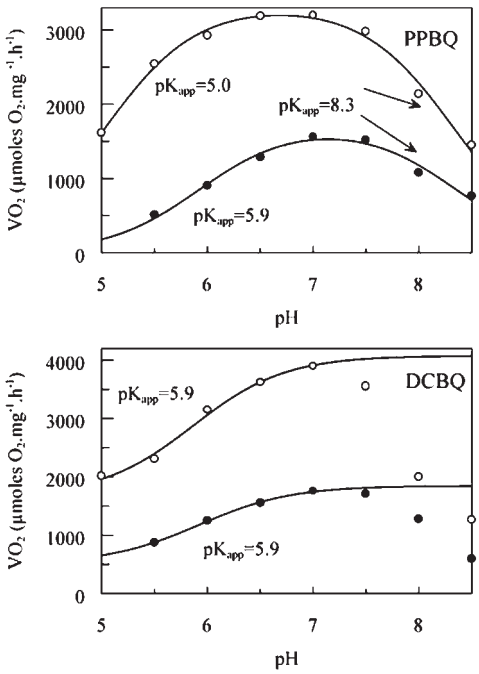

FIG. 7. **Oxygen-evolving activity as a function of pH of calcium-PSII (*open circles*) and strontium-PSII (*filled circles*) in the presence of 0.5 mM PPBQ (*upper panel*) or 0.5 mM DCBQ (*lower panel*).** Chl concentration was 5 μg/ml. Data were fitted using the program Grafit (Erithacus Software) with either bell-shaped curves for activity measurements done in the presence of PPBQ or using a single p*K* for data below pH 8 for activity measurements done in the presence of DCBQ.

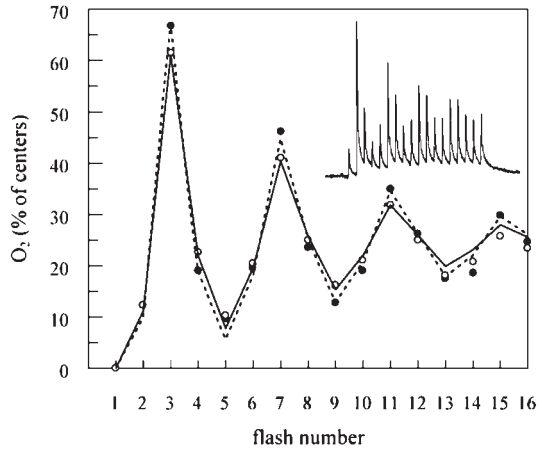

FIG. 8. **Flash-induced oxygen evolution pattern during a sequence of saturating xenon flashes (spaced 400 ms apart) given on Ca-thylakoids (*filled circles*) and Sr-thylakoids (*open circles*).** The samples (Chl = 1 mg/ml) were dark-adapted for 1 h at room temperature on the polarized bare platinum electrode. Amplitude of the flash-induced oxygen evolution has been plotted so that it corresponds directly to the percentage of centers in which O_2 is produced. This has been done by scaling the experimental data to the simulated data obtained as described in the text. The *continuous* and *dashed lines* are the results of the fitting procedure for the Ca-thylakoids and Sr-thylakoids samples, respectively. The S_1/S_0 ratio and α and β parameters used for the fits are described under "Results."

function of pH with either DCBQ or PPBQ as electron acceptors. Because the incubation time in the presence of betaine was very short, DCBQ could be used here. Results are shown in Fig. 7. Best fittings of the data were obtained using bell-shaped curves (with two apparent p*K* values) for measurements in the presence of PPBQ (*panel A*) or curves with a single apparent p*K* for the acidic region in the presence of DCBQ (*panel A*). Several observations can be made: 1) the Ca^{2+}/Sr^{2+} exchange decreased the activity by a factor ≈2.2–2.4; 2) in both PSII preparations, the activity was higher with DCBQ than with PPBQ; 3) the apparent p*K* in the acidic region (p*K* = 5.9) is similar in strontium-PSII and calcium-PSII with DCBQ and strontium-PSII with PPBQ, but is slightly different (p*K* = 5.0) for calcium-PSII with PPBQ; 4) the basic apparent p*K* (p*K* ≈ 8.3) was similar with strontium-PSII and PS/calcium with either PPBQ or DCBQ. These small differences seem unlikely to be caused by a direct effect of the Ca^{2+}/Sr^{2+} exchange in the site.

The stability of the S_n-states in the strontium-containing enzyme has been investigated by using a Joliot-type O_2 electrode. This technique requires the use of thylakoids (or cells) instead of PSII because sedimentation of the sample on the bare platinum electrode is required. An advantage of this kind of experiment is that it is easy to have a complete flash sequence and therefore to calculate from the flash-induced oxygen pattern both the proportions of $S_3/S_2/S_1/S_0$ and the α and β parameters. A complete study comparing properties of Ca-thylakoids from *T. elongatus* with those from plants has been recently performed (70). In particular, the role of Tyr_D and temperature have been investigated. In the present work, we have compared Sr-thylakoids and Ca-thylakoids at room temperature and after a similar dark-adaptation period on the electrode.

Flash-induced O_2 evolution patterns from Sr-thylakoids and Ca-thylakoids samples dark-adapted for 1 h at room temperature on the polarized electrode are shown in Fig. 8. The *inset* in Fig. 8 shows an example of the direct trace obtained with dark-adapted Sr-thylakoids. From the fit of the sequences, the following parameters were obtained: in calcium-PSII: α = 8%, β = 7%, S_1 = 85%, S_0 = 15%; in strontium-PSII: α = 8%, β = 5%, S_1 = 95%, S_0 = 5%.

As observed above, the α and β parameters were found to be similar in Sr-thylakoids and Ca-thylakoids. If significant, the smaller β value in Sr-thylakoids could originate from a slower P^+_{680} reduction by Tyr_Z, as suggested from data in Fig. 5. The percentage of centers in the S_1-state in Sr-thylakoids was found to be higher than in Ca-thylakoids. This observation is easily understandable from the experiments reported below.

The reduction (or "deactivation"), in the dark of the S_3- and S_2-states has been determined. Samples, dark-adapted for 1 h on the electrode, were submitted to two flashes. Then, after a second dark period (the deactivation time), varying from 0.4 s to 90 min, a series of 19 flashes was given. The flash-induced O_2 evolution patterns were measured and fitted, using the same α and β values as above, and the $S_3/S_2/S_1/S_0$ contents after each deactivation time were deduced. The plots of the $S_3/S_2/S_1$ concentrations *versus* the deactivation time in Ca-thylakoids and Sr-thylakoids are shown in Fig. 9 (*A* and *B*), respectively. Results from the fits are listed in Table II. For each sample, the three kinetics were fitted globally using exponential decays and assuming that the deactivation from S_3 to S_1 occurred via S_2 in all centers. A bi-exponential decay was used for the deactivations from S_3 to S_2. The fits also included a proportion of centers in S_2 (which deactivated to form S_1 during the experiment) and a proportion of centers in S_1 after the second flash. The proportion of centers in the S_0-state was considered as negligible after two flashes so that the equation describing the proportion of S_1 as a function of time did not take into account the possible $S_0Tyr_D^{\cdot}$ to S_1Tyr_D reaction. We also neglected a possible fraction of centers in the S_2Tyr_D-state after the second flash, which would give the $S_1Tyr_D^{\cdot}$ state. The equations used are listed below.

$$[S_3]_t = [S_3]_{t=0} \cdot (p \cdot \exp(-k_1 \cdot t) + (1 - p) \cdot \exp(-k_2 \cdot t)) \qquad \text{(Eq. 3)}$$

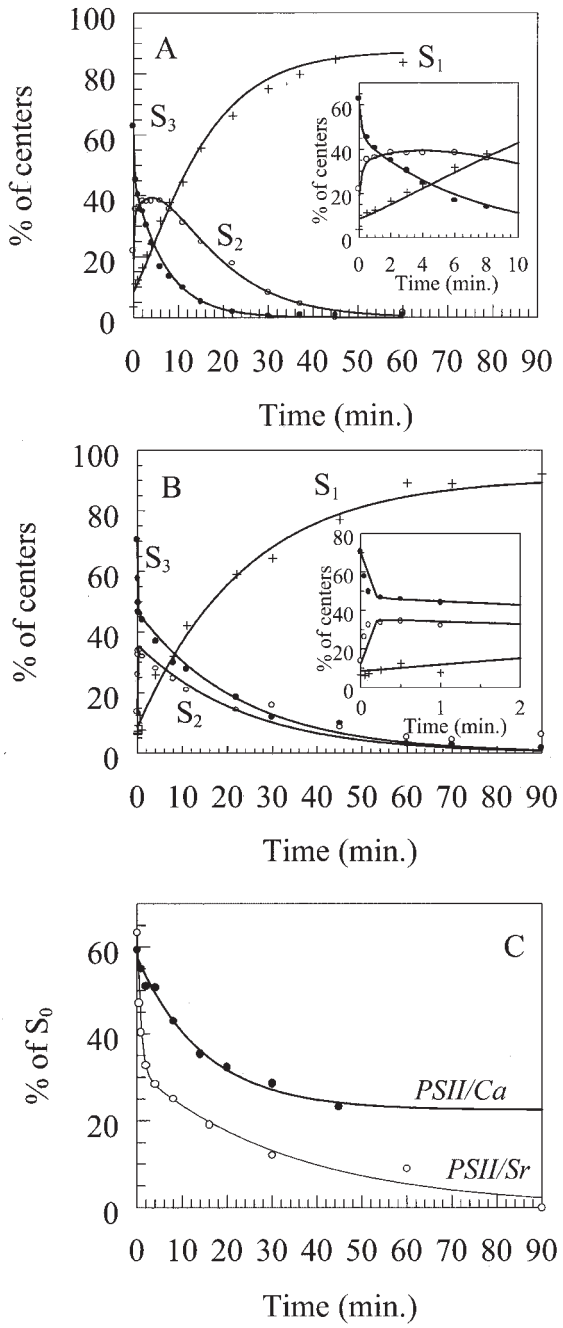

FIG. 9. **Deactivation kinetics of the S_3- and S_2-states and formation of the S_1-state, in the dark, at room temperature, in Ca-thylakoids (*panel A*) and Sr-thylakoids (*panel B*).** *Panel C* shows the kinetics of the S_0-state to S_1-state conversion in Ca-thylakoids (*filled circles*) and Sr-thylakoids (*open circles*). See "Results" for other details.

$$[S_2]_t = [S_2]_{t=0}\cdot\exp(-k_3\cdot t) + p\cdot[S_3]_{t=0}\cdot(k_1/(k_3-k_1)\cdot(\exp(-k_1\cdot t)-\exp(-k_3\cdot t))) + (1-p)\cdot[S_3]_{t=0}\cdot(k_2/(k_3-k_2)\cdot(\exp(-k_2\cdot t)-\exp(-k_3\cdot t))) \quad \text{(Eq. 4)}$$

$$[S_1]_t = [S_1]_{t=0} + [S_2]_{t=0}\cdot(1-\exp(-k_3\cdot t)) + ([S_3]_{t=0} - [S_3]_t - (p\cdot[S_3]_{t=0}\cdot(k_1/(k_3-k_1)\cdot(\exp(-k_1\cdot t)-\exp(-k_3\cdot t))) + (1-p)\cdot[S_3]_{t=0}\cdot(k_2/(k_3-k_2)\cdot(\exp(-k_2\cdot t)-\exp(-k_3\cdot t))))) \quad \text{(Eq. 5)}$$

$[S_3]_t$, $[S_2]_t$, and $[S_1]_t$ were the experimental points and $[S_3]_{t=0}$, $[S_2]_{t=0}$, $[S_1]_{t=0}$, k_1, k_2, k_3, p the variables to adjust.

In both Ca-thylakoids and Sr-thylakoids, the S_3 to S_2 deactivation was found to be biphasic. The fastest phase was 4 times faster in Sr-thylakoids than in Ca-thylakoids. This fast phase ($t_{1/2}$ = 7.8 and 2.4 s) corresponds very probably to the reduction of S_3 into S_2 by Tyr_D. By contrast with a previous work (70), no specific protocol has been used here to have 100% $Tyr_D^{\cdot}$ at the beginning of the experiments. The slow phase for the S_3 reduction to S_2 was found to be almost 4 times slower in strontium-PSII than in calcium-PSII. The rate of S_2 deactivation into S_1 was found to be insensitive to the Sr^{2+} substitution. The monophasic decay in this process probably results from the protocol used. Indeed, any Tyr_D that could have contributed to a fast S_2 decay would have been already oxidized during the S_3 to S_2 deactivation.

The oxidation rate, in the dark, of the S_0-state into the S_1-state was determined using the following protocol. Samples dark-adapted for 1 h (on the electrode) at room temperature were submitted to three flashes. Then, after a second dark period, varying from 0.4 s to 90 min, a series of 19 flashes was given. The flash-induced O_2 evolution patterns were measured and fitted using the deduced $S_3/S_2/S_1/S_0$ concentrations after the varying dark periods. The S_0-state proportions *versus* the varying dark times in Ca-thylakoids and Sr-thylakoids are shown in Fig. 9*C*. The data were fitted using bi-exponential decays.

$$[S_0]_t = [S_0]_{t=0}\cdot(q\cdot\exp(-k_4\cdot t) + (1-q)\cdot\exp(-k_5\cdot t)) \quad \text{(Eq. 6)}$$

In both Ca-thylakoids and Sr-thylakoids, the disappearance of the S_0-state occurred in a biphasic process. In Ca-thylakoids, the slowest phase was considered to be a constant on the time scale used here. As mentioned above, the most obvious origin for the S_0-state decay is the $S_0\ Tyr_D^{\cdot}$ to S_1Tyr_D reaction. This reaction was found to be considerably accelerated in Sr-thylakoids compared with Ca-thylakoids. The higher efficiency of the $S_0Tyr_D^{\cdot}$ to S_1Tyr_D reaction in Sr-thylakoids *versus* Ca-thylakoids could explain the higher proportion of centers in the S_1-state in dark-adapted Sr-thylakoids (and probably also in strontium-PSII).

As shown above, the lower oxygen evolution activity reported in Sr^{2+}-reconstituted Ca^{2+}-depleted PSII is consistent with slower S-state transitions. In particular, both EPR and absorption changes measured at 292 nm indicated that the $S_3Tyr_Z^{\cdot}$ to S_0Tyr_Z transition slows down from ≈1.6 to ≈10 ms. The $S_3Tyr_Z^{\cdot}$ to S_0Tyr_Z transition is that in which the O_2 release occurs. The rate of this oxygen release can be roughly estimated with the electrode used above (71). Such an experiment is depicted in Fig. 10. In this experiment, the oxygen release was measured after the third flash using Sr-thylakoids and Ca-thylakoids dark-adapted for 1 h at room temperature. The $t_{1/2}$ for the oxygen release was estimated to be 1–2 ms in Ca-thylakoids and 5–7 ms in Sr-thylakoids. The O_2 release in Sr-thylakoids was found to be slightly faster than the $S_3Tyr_Z^{\cdot}$ to S_3Tyr_Z transition measured above in strontium-PSII. Effects caused by the detergent used for PSII purification could be at the origin of this slowdown. The integration of the amperometric signal from $t = 0$ (but without the small artifact) to the time where all of the O_2 was consumed by the electrode, gave a similar value in Ca-thylakoids and Sr-thylakoids. This indicates that a similar amount of O_2 has been evolved in both samples. Comparisons between the values found here for the oxygen release and those found above for the $S_3Tyr_Z^{\cdot}$ to S_3Tyr_Z transition show that the latter reaction is the limiting step in the oxygen evolution process.

DISCUSSION

The finding that *T. elongatus* can grow at the same rate in a culture medium containing Sr^{2+} instead of Ca^{2+}, although the

TABLE II
Deactivation kinetics of the S_3- into S_2-states and S_2- into S_1-states and kinetics of oxidation in the dark of the S_0- into S_1-states in Ca-thylakoids and Sr-thylakoids

	$S_3 \rightarrow S_2$		$S_2 \rightarrow S_1$		$S_0 \rightarrow S_1$	
	%	*half-time*	%	*half-time*	%	*half-time*
Ca-thylakoids	76	4.9 min	100	7.5 min	62	9.9 min
	24	7.8 s			38	Constant
Sr-thylakoids	67	16 min	100	7.1 min	50	34 s
	33	2.4 s			50	24 min

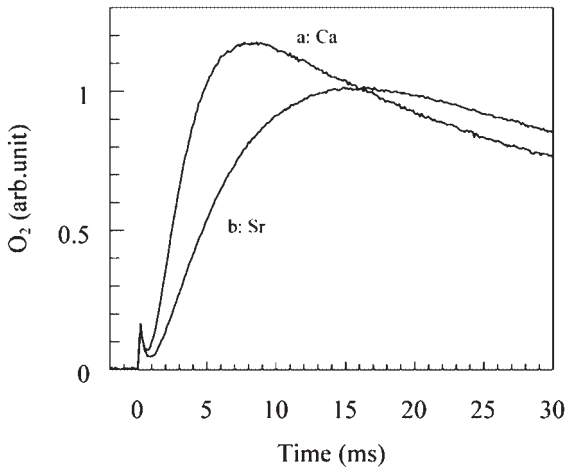

FIG. 10. **Kinetics of the oxygen release measured after the third flash given on Ca-thylakoids (*trace a*) and Sr-thylakoids (*trace b*) dark-adapted for 1 h on the bare platinum electrode.** Other experimental conditions were as in Fig. 8 except that the time scale was 10 times faster.

result we were looking for, was something of a surprise. The observation that the cells died without Sr^{2+} addition shows that Ca^{2+} contamination in the medium could not sustain cell growth. However, in the strontium-grown cells, the Ca^{2+} contamination measured was ~0.5% of that in calcium-grown cells. It seems possible then that other physiological functions, which may be rigorously dependent on Ca^{2+}, could have been satisfied by this Ca^{2+} contamination. From many of the results presented above and discussed below, it is clear the Ca^{2+} requirement in O_2 evolution is completely satisfied by Sr^{2+}. The observation that the cell growth rate is similar in strontium and calcium media, even though the enzyme activity is markedly inhibited, shows that the water oxidation activity does not limit cell growth under the culture conditions used.

The isolation and purification of oxygen-evolving PSII from strontium-grown cells required the presence of betaine in all the media other than the culture medium. Although the protective role of betaine is not fully understood, it has been shown that it protects PSII against the loss of the three extrinsic proteins (61). In the absence of betaine, it appears that the Sr^{2+}/Ca^{2+} exchange decreases the strength of the binding of the extrinsic proteins to PSII. In our earlier work with PSII from plants, we had observed that the reconstitution of the 24- and 17-kDa polypeptides failed when Sr^{2+} had been biochemically substituted for Ca^{2+}.[2] This could reflect the same phenomenon in the PSII from plants. It is, however, surprising that the exchange of a single Ca^{2+} ion with a Sr^{2+} ion within the active site should have the effect of destabilizing the binding properties of the extrinsic polypeptides. Superficially, the new x-ray crystallographic structure does not provide an obvious explanation for this effect (50).

Quantification of Ca^{2+} in biological samples is difficult because the concentration of unspecific Ca^{2+} is often high and it is sometimes impossible to decrease this background below to the concentration of the enzyme. This is particularly true with cyanobacteria, for which the oxygen-evolving activity decreases irreversibly when PSII is resuspended in media with a Ca^{2+} concentration below 10 mM (data not shown, but see Ref. 33). This protective effect of Ca^{2+} is not clearly understood, but it complicates quantification of Ca^{2+} in the enzyme site. The use of PSII with Sr^{2+} in the Ca^{2+} site allowed us to overcome this difficulty. Because strontium-PSII was purified in the presence of 15 mM Ca^{2+} in all buffers, any exchangeable Sr^{2+} ions, either specifically or nonspecifically bound to PSII, were expected to be efficiently exchanged with Ca^{2+} from the buffer. Analysis of the metal content in the isolated strontium-PSII enzyme showed 1 strontium/4 manganese. This highly sequestered strontium ion is responsible for the modification of the enzyme.

Given the nonexchangeability of Sr^{2+}, the loss of activity in media lacking Ca^{2+} seems more likely to be associated with an additional structural role of Ca^{2+} not directly related to that in the active site. This could explain some of the reports in the literature (1, 5, 48) of a different specificity for metal cations in cyanobacterial PSII.

Strontium-PSII isolated in the presence of betaine showed a polypeptide profile on SDS-polyacrylamide gels that was very similar to that of calcium-PSII. In Sr-thylakoids, there was no evidence for inactive centers. Indeed, the amount of O_2 evolved per flash in Sr-thylakoids (*i.e.* equivalent to the amount of active PSII centers, assuming a similar number of Chl/PSII and a similar PSII/PSI ratio in Ca-thylakoids and Sr-thylakoids) was similar to that evolved in Ca-thylakoids. The kinetics of $Tyr_Z^{\cdot}$ reduction measured by EPR gave an upper limit of 5–10% of inactive centers, but the kinetics of $Tyr_Z^{\cdot}$ reduction measured by absorption changes at 292 nm did not exhibit any slow phases that could correspond to $Tyr_Z^{\cdot}$ reduction in manganese-depleted PSII. Furthermore, illumination of strontium-PSII at 200 K gave a negligible amount of chlorophyll cation radical, Chl_Z^{+} (data not shown), a species that is formed at low temperatures when both the manganese cluster and the cytochrome b_{559} are unable to donate electrons (72); hence, the formation of this radical is considered to be a measure of damaged centers.

The lower amplitude of the period of four oscillations in strontium-PSII, measured at 292 nm, compared with those observed in calcium-PSII could be an indication of the presence of 5–10% of inactive centers. Alternatively, it is possible that the Sr^{2+}/Ca^{2+} exchange modifies the $\Delta\epsilon$ of at least some of the S_i to S_{i+1} transitions and this could be responsible for the lower amplitude in the 292 nm oscillations.

It has been reported that the light-driven assembly of the manganese/calcium (manganese/strontium) cluster ("photoactivation") occurs with greater efficiency when $Sr^{2+}$is present instead of Ca^{2+} (6). This effect has been interpreted as originating from a higher binding affinity of Ca^{2+} *versus* Sr^{2+} for hydroxide. Otherwise, the specificity of the Ca^{2+}-depleted enzyme for Sr^{2+} and Ca^{2+} to reconstitute the O_2-evolving activity (73) has been interpreted as originating from the similar p*K* for

[2] A. Boussac, unpublished data.

Sr^{2+} and Ca^{2+} on the Lewis scale. A study of the pH dependence of oxygen evolution in strontium-PSII *versus* calcium-PSII showed no significant differences. Nevertheless, it is of note that we measured the activity under continuous illumination. Thus, if the Sr^{2+}/Ca^{2+} exchange influenced a nonlimiting step in the cycle, it would not have been detected. This might at least partially explain the discrepancy between the apparent p*K* found here and those found earlier (74) for each S-state transition in PSII/calcium. Future work will be aimed at studying the influence of pH on each individual S-states in strontium-PSII compared with calcium-PSII.

O_2 release occurs with a $t_{½}$ close to 1–2 ms in Ca-thylakoids and 5–7 ms in Sr-thylakoids. These kinetics correspond to those of the $S_3Tyr_Z^{\cdot}$ to S_0Tyr_Z transition measured here both by EPR and by absorption changes measurements at 292 nm. This result is in line with the model in which O_2 release is limited by the $S_3Tyr_Z^{\cdot}$ to S_0Tyr_Z transition (65). We had hoped that the strontium substitution may allow for the resolution and even trapping of intermediate states occurring in the water oxidation mechanism on the S_3 to S_0 transition (see, for example, Ref. 75). Further modifications of the enzyme are required before potential intermediates can be resolved.

Given existing knowledge of the enzyme (see Introduction but also Ref. 50), it seems reasonable that the main influence of Sr^{2+} will be on its nearest neighbors, the Tyr_Z and particularly the Mn_4. A slowdown in the forward steps of the enzyme cycle (the advancement of the S-states) and the associated lowering of oxygen-evolving activity, as reported here and earlier, fit with the existing ideas on the location and role of the Ca^{2+}. Indeed, the recent crystal structure shows the close association of calcium with the manganese and the Tyr_Z (50). The additional observations reported here (the acceleration of Tyr_D to S_3 electron donation, the oxidation of S_0 by $Tyr_D^{\cdot}$, the longer S_3 lifetime, the indications of a slight shift in the $Tyr_ZP^+ \leftrightarrow Tyr_Z^{\cdot}P$ equilibrium toward P^+, and the lack of any change in S_2 lifetime despite the change in its EPR signal) can all be rationalized with changes in the properties of Tyr, manganese and the calcium/strontium itself. It is clear, however, that no single straightforward effect (such as a consistent change in the redox potential of the components, a change in the kinetics of the proton movements, a modification in substrate binding or accessibility, etc.) can explain all the phenomena. It seems likely that one or more of these effects do occur but that they are dependent on the redox state of the enzyme cycle. This is not so surprising because calcium binding and thus calcium ligation seems to be markedly S-state-dependent (76). However, at this point, we cannot rule out an influence of the strontium/calcium exchange on more distant cofactors (such as Tyr_D or Q_A), which could also influence the kinetics of the reaction tested. Future studies will address these problems, focusing on the S-state dependence of the effects.

This work shows that (i) the site of Sr^{2+} in Sr-thylakoids and strontium-PSII is the same as that in Sr^{2+}-reconstituted Ca^{2+}-depleted PSII in plants and (ii) the Sr^{2+}-induced modifications already reported were not a consequence of side effects of the biochemical treatments used. Consequently, there is no reason to question results in the literature deduced from biochemical Sr^{2+}/Ca^{2+} exchange on these grounds; thus, we can assume that this site and that proposed in the recent crystal structure (50) are one and the same. Three of the most important advantages of the strontium-PSII preparation described here over the previously used Sr^{2+}-reconstituted, Ca^{2+}-depleted PSII are the high activity, the high stability, and the homogeneity of the enzyme. This strontium-PSII will be useful for a wide range of enzymological and spectroscopic studies, several of which are under way.

Acknowledgments—We acknowledge Jean Lavorel and Jérôme Lavergne for many discussions and Jean-Marc Ducruet for unpublished thermoluminescence experiments.

Addendum—While this article was in preparation, a new crystallographic model appeared for the active site of PSII (50). This work proposed that the cluster is made up of a Mn_3CaO_4 distorted cubane structure with the 4th manganese linked to one of the oxo groups of the cubane. This confirms that calcium is closely associated with the manganese and indeed is the closest atom of the cluster to the Tyr_Z (50).

REFERENCES

1. Debus, R. J. (1992) *Biochim. Biophys. Acta* **1102,** 269–352
2. Peloquin, J. M., and Britt, R. D. (2001) *Biochim. Biophys. Acta* **1503,** 96–111
3. Barber, J. (2002) *Curr. Opin. Struct. Biol.* **12,** 523–530
4. Robblee, J. H., Cinco, R. M., and Yachandra, V. K. (2001) *Biochim. Biophys. Acta* **1503,** 7–23
5. Yocun, C. F. (1991) *Biochim. Biophys. Acta* **1059,** 1–15
6. Ananyev, G. A., Zaltsman, L., Vasko, C., and Dismukes, G. C. (2001) *Biochim. Biophys. Acta* **1503,** 52–68
7. Boussac, A., and Rutherford, A. W. (1988) *Biochemistry* **27,** 3476–3483
8. Ghanotakis, D. F., Babcock, G. T., and Yocum, C. F. (1984) *FEBS Lett.* **167,** 120–130
9. Jegerschold, C., Rutherford, A. W., Mattioli, T. A., Crimi, M., and Bassi, R. (2000) *J. Biol. Chem.* **275,** 12781–12788
10. Boussac, A., and Rutherford, A. W. (1992) *Photosynth. Res.* **32,** 207–209
11. Adelroth, P., Lindberg, K., and Andréasson, L.-E. (1995) *Biochemistry* **34,** 9021–9027
12. Van der Meulen, K. A., Hobson, A., and Yocum, C. F. (2004) *Biochim. Biophys. Acta*, in press
13. Vrettos, J. S., and Brudvig, G. W. (2002) *Phil. Trans. R. Soc. London B* **357,** 1395–1404
14. Boussac, A., Sétif, P., and Rutherford, A. W. (1992) *Biochemistry* **31,** 1224–1234
15. Westphal, K. L., Lydakis-Simantiris, N., Cukier, R. I., and Babcock, G. T. (2000) *Biochemistry* **39,** 16220–16229
16. Boussac, A., Zimmermann, J.-L., and Rutherford, A. W. (1989) *Biochemistry* **28,** 8984–8989
17. Boussac, A., Zimmermann, J.-L., Rutherford, A. W., and Lavergne, J. (1990) *Nature* **347,** 303–306
18. Gilchrist, M. L., Ball, J. A., Randall, D. W., and Britt, R. D. (1995) *Proc. Natl. Acad. Sci. U. S. A.* **92,** 9545–9549
19. Tang, X. S., Randall, D. W., Force, D. A., Diner, B. A., and Britt, R. D. J. (1996) *J. Am. Chem. Soc.* **118,** 7638–7639
20. Voelker, M., Eckert, H. J., and Renger, G. (1987) *Biochim. Biophys. Acta* **890,** 66–76
21. Haumann, M., and Junge, W. (1999) *Biochim. Biophys. Acta* **1411,** 121–133
22. Rutherford, A. W. (1989) *Trends Biochem. Sci.* **14,** 227–232
23. Pecoraro, V. L., Baldwin, M. J., Caudle, M. T., Hsieh, W. Y., and Law, N. A. (1998) *Pure App. Chem.* **70,** 925–929
24. Vrettos, J. S., Limburg, J., and Brudvig, G. W. (2001) *Biochim. Biophys. Acta* **1503,** 229–245
25. Cinco, R. M., Robblee, J. H., Rompel, A., Fernandez, C., Yachandra, V. K., Sauer, K., and Klein, M. P. (1998) *J. Phys. Chem. B* **102,** 8248–8256
26. Cinco, R. M., Holman, K. L. M., Robblee, J. H., Yano, J., Pizarro, S. A., Bellacchio, E., Sauer, K., and Yachandra, V. K. (2002) *Biochemistry* **41,** 12928–12933
27. Boussac, A., Sugiura, M., Inoue, Y., and Rutherford, A. W. (2000) *Biochemistry* **39,** 13788–13799
28. Britt, R. D., Campbell, K. A., Peloquin, J. M., Gilchrist, M. L., Aznar, C. P., Dicus, M. M., Robblee, J., and Messinger, J. (2004) *Biochim. Biophys. Acta*, in press
29. Chu, H.-A., Sackett, H., and Babcock, G. T. (2000) *Biochemistry* **39,** 14371–14376
30. Kimura, Y., Hasegawa, K., and Ono, T.-A. (2002) *Biochemistry* **41,** 5844–5853
31. Hendry, G., and Wydrzynski, T. (2003) *Biochemistry* **42,** 6209–6217
32. Kodera, Y., Hara, H., Astashkin, A. V., Kawamori, A., and Ono, T.-A. (1995) *Biochim. Biophys. Acta* **1232,** 43–51
33. Pauly, S., Schloddler, E., and Wit, H. T. (1992) *Biochim. Biophys. Acta* **1099,** 203–210
34. Shen, J.-R., Satoh, K., and Katoh, S. (1988) *Biochim. Biophys. Acta* **933,** 358–364
35. Han, C.-H., and Katoh, S. (1993) *Plant Cell Physiol.* **34,** 585–593
36. Olesen, K., Andreasson, L.-E., (2003) *Biochemistry* **42,** 2025–2035
37. Boussac, A,., and Rutherford, A. W. (1995) *Biochim. Biophys. Acta* **1230,** 195–201
38. Shen, J.-R., and Katoh, S. (1991) *Plant Cell Physiol.* **32,** 439–446
39. Diner, B. A. (2001) *Biochim. Biophys. Acta* **1503,** 147–163
40. Debus, R. J. (2001) *Biochim. Biophys. Acta* **1503,** 164–186
41. Sugiura, M., Inoue, Y. (1999) *Plant Cell Physiol.* **40,** 1219–1231
42. Noguchi, T., and Sugiura, M. (2002) *Biochemistry* **41,** 15706–15712
43. Boussac, A., Kuhl, H., Ghibaudi, E., Rögner, M., and Rutherford, A. W. (1999) *Biochemistry* **38,** 11942–11948
44. Boussac, A., Kuhl, H., Un, S., Rögner, M., and Rutherford, A. W. (1998) *Biochemistry* **37,** 8995–9000
45. Kretschmann, H., Schlodder, E., and Witt, H. T. (1996) *Biochim. Biophys. Acta* **1274,** 1–8
46. Zouni, A., Witt, H. T., Kern, J., Fromme, P., Krauss, N., Saenger, W., and Orth, P. (2001) *Nature* **409,** 739–743
47. Kamiya, N., and Shen, J. R. (2003) *Proc. Natl. Acad. Sci. U. S. A.* **100,** 98–103
48. Becker, D. W., and Brand, J. J. (1985) *Plant Physiol.* **79,** 552–558
49. Enami, I., Iwai, M., Akiyama, A., Suzuki, T., Okumura, A., Katoh, T., Tada, O.,

Ohta, H. S. (2003) *Plant Cell Physiol.* **44,** 820–827
50. Barber, J., Norell, K., Iverson, T., Maghlaoui, K., and Iwata, S. (2004) *Science* **303,** 1831–1838
51. Porra, R. J. (1991) in *The Chlorophylls* (Scheer, H., ed) pp. 31–57, CRC Press, Boca Raton, FL
52. Ikeuchi, M., and Inoue, Y. (1988) *Plant Cell Physiol.* **29,** 1233–1239
53. Miyao, M., Murata, N., Lavorel, J., Maison, B., Boussac, A., and Etienne, A.-L. (1987) *Biochim. Biophys. Acta* **890,** 151–159
54. Boussac, A., Un, S., Horner, O., and Rutherford, A. W. (1998) *Biochemistry* **37,** 4001–4007
55. Béal, D., Rappaport, F., and Joliot, P. (1999) *Rev. Sci. Instr.* **70,** 202–207
56. Carrier, P., Baryla, A., and Havaux, M. (2003) *Planta* **216,** 939–950
57. Karnovski, M. J. (1971) *Am. Soc. Cell Biol.* **284,** 146A
58. Schultze-Lam, S., and Beveridge, T. J. (1994) *Appl. Environ. Microbiol.* **60,** 447–453
59. Douglas, S. (1998) *Can. J. Microbiol.* **44,** 128–139
60. Roncel, M., Boussac, A., Zurita, J. L., Bottin, H., Sugiura, M., Kirilovsky, D., and Ortega, J.-M. (2003) *J. Biol. Inorg. Chem.* **8,** 206–216
61. Chen, T. H. H., and Murata, N. (2002) *Curr. Opin. Plant Biol.* **5,** 250–257
62. Kuhl, H., Rögner, M., van Breemen, J. F. L., and Boekema, E. J. (1999) *Eur. J. Biochem.* **266,** 453–459
63. Zimmermann, J.-L., and Rutherford, A. W. (1986) *Biochim. Biophys. Acta* **851,** 416–423
64. Lavergne, J., (1991) *Biochim. Biophys. Acta* **1060,** 175–188
65. Rappaport, F., Blanchard-Desce, M., and Lavergne, J. (1994) *Biochim. Biophys. Acta* **1184,** 178–192
66. Lavorel, J. (1978) *J. Theor. Biol.* **57,** 171–185
67. Razeghifard, M. R., and Pace, R. J. (1997) *Biochim. Biophys. Acta* **1322,** 141–150
68. Dekker, J. P., Ghanotakis, D. F., Plijter, J. J., van Gorkom, H. J., and Babcock, G. T., (1984) *Biochim. Biophys. Acta* **767,** 515–523
69. Yerkes, C. T., and Babcock, G. T. (1981) *Biochim. Biophys. Acta* **634,** 19–29
70. Isgandarova, S., Renger, G., and Messinger, J. (2003) *Biochemistry* **42,** 8929–8938
71. Lavorel, J. (1992) *Biochim. Biophys. Acta* **1101,** 33–40
72. Stewart, D. H., and Brudvig, G. W. (1998) *Biochim. Biophys. Acta* **1367,** 63–87
73. Vrettos, J. S., Stone, D. A., and Brudvig, G. W. (2001) *Biochemistry* **40,** 7937–7945
74. Bernat, G., Morvaridi, F., Feyziyev, Y., and Styring, S. (2002) *Biochemistry* **41,** 5830–5843
75. Clausen, J., Debus, R. J., and Junge, W. (2004) *Biochim. Biophys. Acta*, in press
76. Boussac, A., and Rutherford, A. W. (1988) *FEBS Lett.* **236,** 432–436